Additive Manufacturing 13 (2017) 143–148

Contents lists available at ScienceDirect

Additive Manufacturing

journal homepage: www.elsevier.com/locate/addma

Original Research Article

3D inkjet-printed UV-curable inks for multi-functional electromagnetic applications

Ehab Saleh[a,*], Peter Woolliams[b], Bob Clarke[b], Andrew Gregory[b], Steve Greedy[c], Chris Smartt[c], Ricky Wildman[a], Ian Ashcroft[a], Richard Hague[a], Phill Dickens[a], Christopher Tuck[a]

[a] Additive Manufacturing and 3D Printing Research Group, University of Nottingham, Nottingham, NG7 2RD UK
[b] The National Physical Laboratory (NPL), Teddington, TW11 0LW, UK
[c] George Green Institute for Electromagnetics Research, University of Nottingham, Nottingham, NG7 2RD, UK

ARTICLE INFO

Article history:
Received 29 April 2016
Received in revised form 19 August 2016
Accepted 10 October 2016
Available online 14 October 2016

Keywords:
3D inkjet printing
UV curable ink
Iron oxide ink
Electromagnetic
Additive manufacturing

ABSTRACT

Inkjet printing of multiple materials is usually processed in multiple steps due to various jetting and curing/sintering conditions. In this paper we report on the development of all inkjet-printed UV-curable electromagnetic responsive inks in a single process, and the electromagnetic characterization of the developed structure. The ink consists of iron oxide (Fe_3O_4) nanoparticles (nominal particle size 50–100 nm) suspended within a UV curable matrix resin. The viscosity and surface tension of the inks were tuned to sit within the inkjet printability range.

Multiple layers of the electromagnetic active ink were printed alongside passive UV-curable ink in a single manufacturing process to form a multi-material waffle shape. The real permittivity of the cured passive ink, active ink and waffle structure at a frequency of 8–12 GHz were 2.25, 2.73 and 2.65 F/m, respectively. This shows the potential of additive manufacturing (AM) to form multi-material structures with tunable electromagnetic properties.

1. Introduction

Tailored electromagnetic responsive materials have been used in low observable and cloaking applications in the microwave range for many years [1–4]. The type of material and the geometry of the structure are key elements in manipulating the electromagnetic response of the fabricated structure. Being able to fabricate such structures directly from a computer aided design (CAD) will simplify the process of tailoring the electrical and electromagnetic properties of the structure taking advantage of the many recent advances in 3D printing technologies [5–11].

Inkjet printing has been in use for prototyping and manufacturing purposes for around five decades owing to its versatility of depositing various inks with a wide range of properties [12–16]. Although inkjet printing has mostly been used in the graphics industry, recent reports have shown the potential to use inkjet printing in areas like printed electronic [15,17–24], printed optics [25–27] and medical applications [28–32].

This versatility of inks that can be jetted requires different methods of curing for different types of ink. For instance, precursor conductive inks are usually cured by heat to evaporate the binding liquid of the ink and sinter the particles to form conductive films [15,18–20]. Polymeric dielectrics, on the other hand, can be cured using many technologies; one of the most popular methods is by UV irradiation [33,34].

In order to inkjet-print multi-functional materials at least two inks are required with intrinsic differences in their properties. This requires different curing methods for each ink, which does not occur as a problem in traditional 2D printing, but is a major challenge in 3D printing. Each layer in 3D printing can require different post processing methods, for example heating the deposit in an oven or curing within a UV chamber, making the process impractical.

To overcome this challenge, this study used two UV curable inks that were cured in real-time during the printing process to enable the production of multi-material 3D structures in a single deposition process. One ink was a commercial UV curable ink that was used as the passive structural material. The second ink was an active electromagnetic responsive ink that was developed by the authors. The viscosity and surface tension of the active electromag-

* Corresponding author.
E-mail address: Ehab.Saleh@nottingham.ac.uk (E. Saleh).

http://dx.doi.org/10.1016/j.addma.2016.10.002

netic responsive ink were measured to achieve stable printability, different patterns were printed and demonstrated successfully.

Recent studies have taken a similar approach to 3D print conductive tracks by loading UV curable resins with conductive nanoparticles to achieve a percolation of the particles to form a complete conductive path within a resin [35–37]. Sangermano [35] and Chiolerio [36] used silver nanoparticles in poly(ethylene glycol) diacrylate (PEGDA) to form a UV curable conductive ink. Gelves et al. reported a similar concept of using copper and silver nanowires forming polystyrene composites [37]. The electrical conductivity in those reports was limited by the amount of metal load that can be added to the resin hence usually the conductivity is orders of magnitude lower than the bulk metal material. In this study for electromagnetic applications, the active nanoparticle filler is not required to percolate to manipulate the electromagnetic response therefore encapsulating the nanoparticles within the UV resin is feasible.

Song et al. [38] inkjet printed a solvent-based magnetic ink onto commercial inkjet paper which quickly absorbed the solvent of the ink. The approach showed excellent magnetic properties but was restricted to only 2D applications. Nardi et al. [39] have formulated a magnetic responsive composite of iron oxide (Fe_3O_4) dispersed in a UV curable acrylic resin. However, the composite material was not used in an inkjet printing application though it showed the potential of using the composite formula in electromagnetic applications. Another approach to form electromagnetic responsive jettable inks by Jacot-Descombes et al. [40] was conducted by using a thermal crosslinker instead of UV crosslinker with iron oxide nanoparticles dispersed in a monomer. The aim of this approach was to print thick layers which could not be achieved with UV photoinitiators due to UV absorption by the iron oxide thus restricting the UV method to only thin layers. Whilst the approach was novel for its purpose the thermal crosslinking took excessive time and temperatures, three hours at 160 °C, to form 88.8 μm layers, which is not suitable for applications where layer by layer deposition is preferred, as these conditions would lead to excessive print times. Grant et al. and Shemelya et al. conducted two different studies using spray deposition, casting [41] and filament extrusion [41,42] to manufacture electromagnetic responsive structures. Although spray deposition and casting are rapid and inexpensive techniques they require masks and molds to form different patterns, limiting flexibility and ultimately geometric complexity. Extrusion, on the other hand, is suitable for producing various structures from CAD and has a potential to support higher loadings and the resulting higher viscosities, however the method is restricted to low resolutions when compared to inkjet printing techniques.

In this work, the electromagnetic properties of a UV curable polymeric passive ink and a UV curable iron oxide-doped active ink were characterized at frequencies ranging from 8 GHz to 13 GHz. The characterization also included a 'waffle' shape structure containing the active and passive ink, which showed intermediate properties between the two parent inks. Those results were also reverse-engineered to compute the electromagnetic properties of the materials. Those properties can be used in future studies to simulate the RF frequency response as the structure of the materials is varied. In order to highlight this, the experimentally obtained material properties were used to set up an electromagnetic, full field time domain simulation of the printed structures to provide a complete RF analysis.

2. Experimental section

2.1. Materials

The UV curable dielectric ink was EMD6415 from SunChemical. Iron oxide (Fe_3O_4) nanoparticles were 50–100 nm in diameter from Sigma-Aldrich (SKU: 637106). To reduce the viscosity of the developed active ink a diluent, ethylene glycol dimethacrylate (EGD), from Sigma-Aldrich (SKU: 335681) was used with the final ink as shown in Table 1. A surfactant from ALTANA (BYK-UV-3570) was also used in order to disperse the nanoparticles well within the ink. Glass microscope slides and polyethylene terephthalate (PET) films were used as the substrates in all experiments.

2.2. Ink formulation

To formulate the active ink, 5, 10 and 20 wt% of iron oxide (Fe_3O_4) nanoparticles were added to the EMD6415 UV curable dielectric which acts as a matrix liquid in which to suspend the nanoparticles. To disperse the nanoparticles the precursor was sonicated in an ultrasonic bath for three hours at 40 °C. To reduce the viscosity of the ink 2 wt% of the diluent ethylene glycol dimethacrylate was added to the EMD6415 UV curable resin. An addition of 3 wt% of BYK-UV-3570 surfactant was made to the EMD6415 in order to sustain a well-dispersed nanoparticle ink during printing. Table 1 shows a summary of the different configuration of the inks investigated.

To optimize the ink properties for printing, the liquid (BinderA) was used as an optimal binder solution, hence two final active inks were developed as shown in Table 2 using 5 wt% and 10 wt% of iron oxide nanoparticles suspended in 95 wt% and 90 wt% of BinderA, respectively.

To characterize the inks a Malvern Kinexus Pro rheometer was used to measure the viscosity and a Krüss DSA100 to measure the surface tension using the pendant drop method. Printing of the inks was conducted using a dual-head PixDro LP50 inkjet printer fitted with two Fuljifilm Spectra 128SE piezo electric printheads.

3. Results

3.1. Ink characterization

To be able to assess the printability of the active ink, viscosity, density and surface tension were measured. The viscosities of all inks in Table 1 were measured against temperature as shown in Fig. 1a.

The viscosity of UV80-Fe20 containing 20 wt% of iron oxide was too high for inkjet applications (i.e. <20cP) hence experiments using this load percentage were not continued. Also high loading of nanoparticles can reduce the amount of UV penetration through the resin due to optical absorption, therefore printing was conducted on the ink which contains 10 wt% of iron oxide nanoparticles. The optimized binding liquid (BinderA) containing the UV curable resin with diluent and surfactant was used to form the final active inks using 5 wt% and 10 wt% of iron oxide. The viscosities of

Table 1
Initial formulation of the inks and the binder liquid.

Ink	EMD6415 UV [wt%]	Iron oxide [wt%]	EGD [wt%]	BYK-UV-3570 [wt%]
UV95-Fe5	95	5	0	0
UV90-Fe10	90	10	0	0
UV80-Fe20	80	20	0	0
UV98-D2	98	0	2	0
BinderA	95	0	2	3

Table 2
Material matrices of the active inks.

Ink	BinderA [wt%]	Iron oxide [wt%]
BinderA95-Fe5	95	5
BinderA90-Fe10	90	10

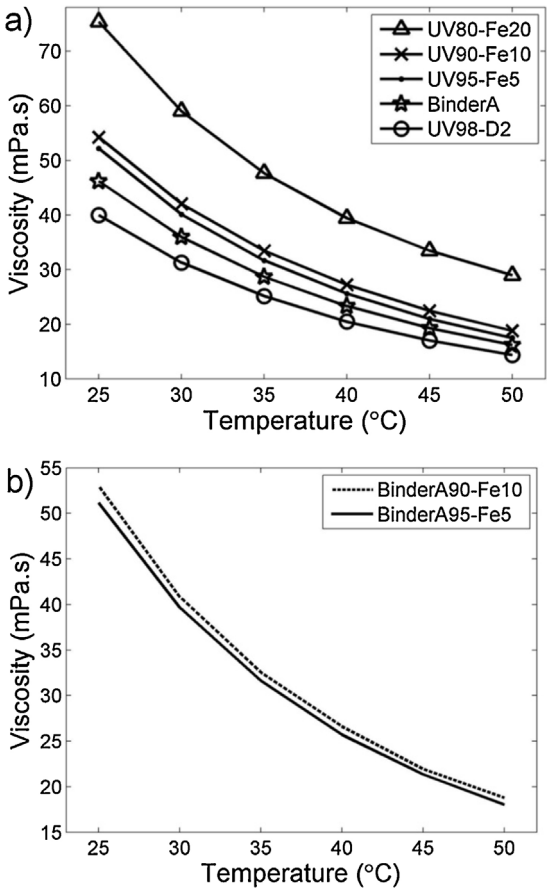

Fig. 1. Viscosities of a) the inks shown in Table 1 changing with temperature, b) the optimized active inks shown in Table 2.

Table 3
Density, surface tension and viscosity of the optimized active inks.

Ink	Density [g/mL]	Surface tension [mN/m]	Viscosity at 50 °C [mPa.s]
BinderA95-Fe5	1.14523	23.91	18.03
BinderA90-Fe10	1.19573	20.91	18.80

the active inks shown in Table 2 (BinderA95-Fe5 and BinderA90-Fe10) were also measured at temperatures ranging from 25 °C to 50 °C as shown in Fig. 1b.

The density and surface tension of the active inks BinderA95-Fe5 and BinderA90-Fe10 were also measured to evaluate the printability of the inks. Density was measured using the Archimedes principle and the surface tension was measured using the pendant method (DSA100) from Krüss. Table 3 shows a summary of the density, the surface tension and the viscosity at 50 °C of the optimized active inks.

The surface tension of the EMD6415 UV resin was 33.13 mN/m, however when a surfactant (3 wt%) was added the surface tension was dropped to 23.77 mN/m. This value is close to the surface tension value of the BinderA95-Fe5 ink, which highlights that 5 wt% loading of nanoparticles didn't provide any significant change to the surface tension of the undoped UV curable resin.

3.2. Printed samples

Printing the optimized active inks alongside the UV curable passive ink (containing no metal particles) was conducted using a dual-head PixDro LP50 inkjet printer. The inks were loaded into the ink reservoirs and purged towards 35 μm orifice diameter nozzles. The voltage of the piezoelectric driven print-heads was set to 100–105 V at each nozzle, and the temperature of the print-head was set to 50 °C in order to operate at relatively low viscosity. Printing resolution was set to 508 dpi which corresponds to a 50 μm drop spacing. This resolution was determined based on the measurement of the average droplet size on a glass substrate (70–75 μm) which provides 30-–35% overlap between the droplets. The average layer thickness of the active and passive inks was determined by measuring the thickness of 300 layers samples and dividing the total thickness of the samples by the number of layers. Both inks showed an average layer thickness of 10.3 ± 0.2 μm. UV curing was conducted in real time using a high power UV LED Phoseon Firefly 28438 (395 nm radiation, 4 W/cm^2) attached to the print-head as shown in Fig. 2a.

Prior to conducting each print, the active ink container was sonicated for 30 min to disperse the nanoparticles thoroughly in the binder liquid. Initial prints were conducted using the active ink only to assess its printability. Multiple layers of the 10 wt% of iron oxide active ink were printed and UV cured forming an array of cells each 1×1 mm as shown in Fig. 2b.

For electromagnetic characterization, a waffle shape pattern containing the active BinderA90-Fe10 ink and the passive UV curable ink was printed on PET substrate as shown in Fig. 2c and d.

4. Discussion

4.1. Ink printability

The manipulation of the ink properties, particularly viscosity, was required to achieve good printability of the ink. The Ohnesorge number (*Oh*) [43] is a non-dimensional indicator to evaluate the

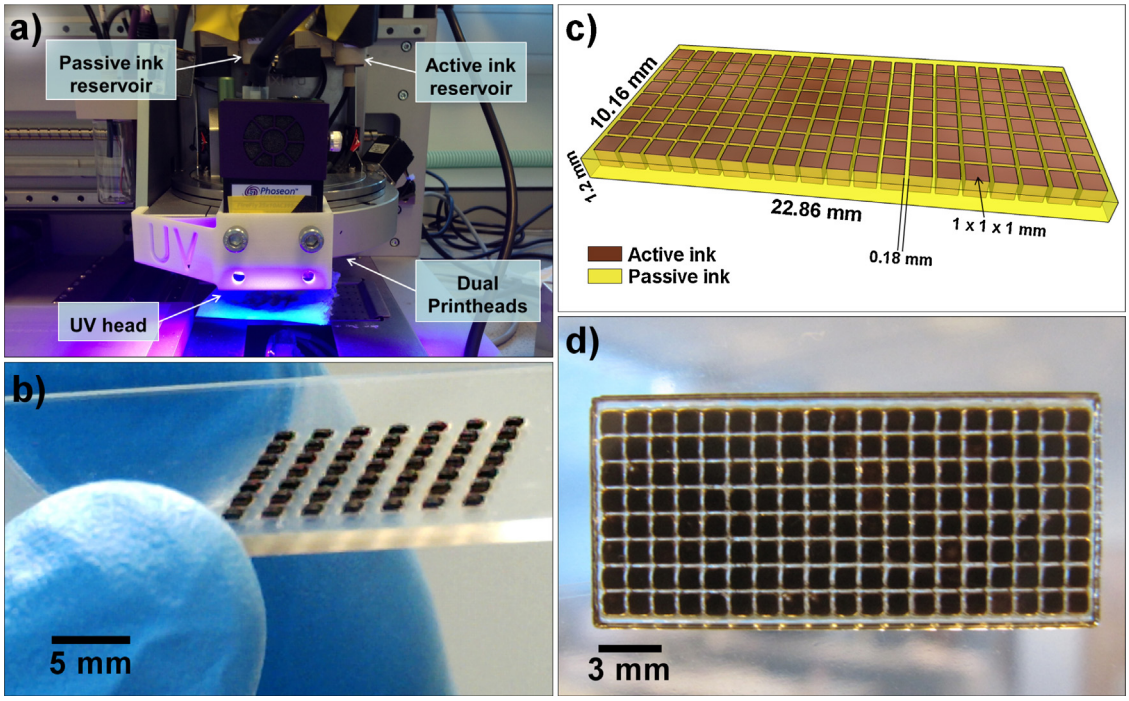

Fig. 2. a) Dual-head PixDro LP50 printer with UV head attached to the head for real time UV curing. b) Multiple layers of UV cured 10 wt% iron oxide active ink printed on a glass substrate. c) The geometry of the waffle shape structure for electromagnetic characterization, d) printed waffle shape sample of the active and passive inks printed on a PET substrate using the LP50 dual-head printer.

printability of an ink, which describes the ratio of internal viscosity dissipation to the surface tension energy as shown in Eq. (1).

$$Oh = \mu/(\rho g D)^{0.5} \quad (1)$$

where μ is the viscosity, ρ is the density, γ is the surface tension and D is the diameter of the nozzle from which the liquid is ejected. The inverse of the Ohnesorge number, known as the Z number, can be used to quantify printability. Although the value of a printable Z number is still under investigation [44,45] inks of Z values $1 < Z < 10$ are considered to be in the printable range [46,47]. In this study, the value of the Z number for the active inks BinderA95-Fe5 and BinderA90-Fe10 at 50 °C is 1.72 and 1.57 respectively.

We also noticed an occurrence of sedimentation, particularly when inks were left unmoved for a few days, when a separation appears where iron oxide nanoparticles sediment at the bottom of the ink container. Despite using a surfactant, sedimentation could not be completely avoided so ultrasonic mixing of the ink prior to conducting any printing was always required to provide a well-dispersed ink where nanoparticle agglomeration and sedimentation were avoided. This had two benefits; one is on the printing process to avoid blocking the nozzles as a result of sedimentation, and the other is on the electromagnetic properties, where agglomeration of nanoparticles will form pockets of iron oxide separated by larger volumes of polymeric resin, this could resonate at certain frequencies and affect the electromagnetic properties.

4.2. Electromagnetic characterization

The waffle shape samples shown in Fig. 2c and d were designed to be stacked in a standard size rectangular metallic waveguide: WG16 for 8.2–12.4 GHz. The waveguide transmission cell method [48] was used to measure the samples.

The microwave S-parameter measurements on the cell and samples were made on a Rhode and Schwarz ZVB Vector Network Analyzer (VNA). The samples were measured in transmission and reflection by placing them inside a section of waveguide connected to the network analyzer via adaptors and coaxial cables. A calibration of the VNA was performed by measuring short circuits, a through line and a section of waveguide of known length. A validation check measurement was carried out using a sample of YAG (yttrium aluminum garnet) crystal, which has accurately known microwave properties and is used as a standard reference material. To make the measurements more accurate 3–4 identical samples were stacked together and measured as a unit, the results being the average properties of this.

The waveguide data processing was performed using Python routines which apply the calibration corrections to the measurement data, derive the dielectric properties (transmission permittivity and permeability) of the samples and also derive measurement uncertainties. For homogeneous isotropic dielectrics, limiting uncertainties are usually those of the dimensions of the sample and their measurement. Fig. 3a shows the real permittivity of the undoped passive ink, doped 10 wt% active ink and the waffle shape samples.

The average permittivity of the passive and active loaded inks (10 wt% iron oxide) was 2.25 and 2.73 F/m, respectively. The real permittivity of the waffle shape samples was around 2.65. This value can be tuned between the values of the doped and undoped inks by altering the dimensions of the waffle cells and the percentage between the two inks. The permeability of all inks at a frequency 8–12 GHz was 1 H/m and thus the permeability of the passive ink was unaffected by the doping.

While this is a modest change in the dielectric properties it demonstrates the ability to tune the permittivity using a composite structure using other functional inks. To our knowledge this is an unprecedented approach to inkjet-print two materials in a single process to form 3D electromagnetic tunable structure. For wider application of this approach inks with greater permittivity will be needed, this is the subject of current ongoing research.

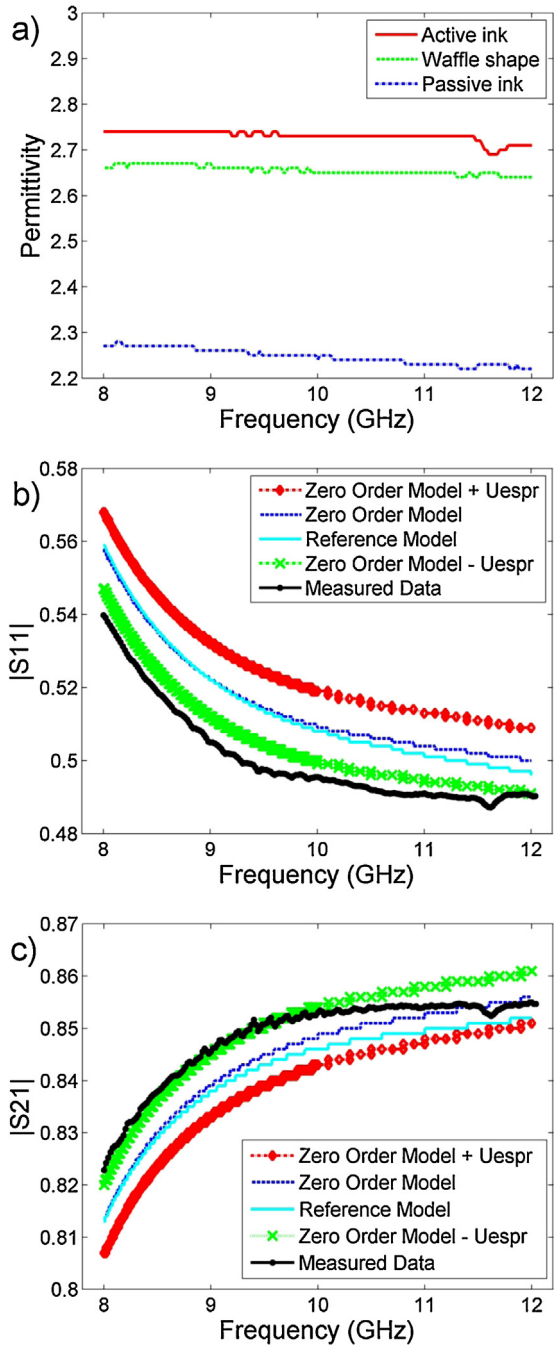

Fig. 3. a) The real permittivity of the cured passive undoped ink and active doped ink as well as the real permittivity of the waffle shape sample as it changes with frequency. b) Simulated reflection coefficients using: (1) a frequency dependent material model, (2) averaged material properties, (3) average materials properties +measurement uncertainty (Uepsr) and (4) average materials properties −measurement uncertainty (Uepsr). c) Simulated transmission coefficients using: (1) a frequency dependent material model, (2) averaged material properties, (3) average materials properties +measurement uncertainty (Uepsr) and (4) average materials properties −measurement uncertainty (Uepsr).

4.3. Electromagnetic simulation

The electromagnetic properties, specifically the permittivity of the materials obtained through measurement were used to define a simulation scenario to determine the scattering parameters in the same manner as that used in the experimental approach.

The simulations were performed using a suite of software tools developed at the University of Nottingham, which are freely available as an open source project [49]. The software is based upon The Transmission Line Matrix (TLM) method of Electromagnetic Field simulation [50], which is a Time Domain method for modelling 3D electromagnetic field interactions with complex structures that can include complex material systems and types. For example: dielectric, magnetic and conducting materials. The software allows for the complete numerical simulation along with post processing and visualization of the problem scenario and results.

The simulations were run across the same frequency range as the experimental process. A number of material models to described the printed structures were developed using the experimentally acquired data, namely: (1) a fully frequency dependent model, (2) a model with constant (average) values of the dielectric properties measured for each material, (3) a model as 2 but with a measurement uncertainty (Uepsr) added to the average values and lastly (4) as 2 but with the measurement uncertainty (Uepsr) subtracted from the average values. The results obtained for the reflection (Fig. 3b) and transmission (Fig. 3c) coefficients are presented along with the experimentally measured data.

Simulated and experimentally measured results show good agreement and provided confidence that the material properties obtained could be used in the design and optimization of further structures to obtain materials with the required frequency response.

In this report iron oxide nanoparticles were printed as part of a UV curable ink, this opens up further investigations to include other organic and inorganic nanoparticles to form UV curable functional inks. Higher loading of nanoparticles could be also considered providing higher intensity of UV irradiation to increase the penetration of light into the sample, and also different deposition methods to eject higher viscosity inks (i.e. PicoDot by Nordson).

We believe this approach can be used to form inks with tailored magnetic, electrical and mechanical properties, yet exhibit similar UV curing characteristics. This approach will facilitate the fabrication of low observable materials, giving enhanced design freedom for building complex structures such as split-ring resonators and triangular resonator for RF metamaterial applications.

5. Conclusion

Iron oxide (Fe_3O_4) nanoparticles of 50–100 nm diameter were dispersed in a UV curable binding liquid to form an active functional UV curable precursor ink. The binding liquid was formed of 95 wt% of a commercial SunChemical UV curable dielectric ink with 2 wt% of a diluent to reduce the viscosity of the liquid and 3 wt% of a surfactant to help disperse nanoparticles in the binding liquid.

The viscosity, density and surface tension of the active inks were optimized to allow for good printability, where the non-dimensional Z number of the 5 wt% iron oxide to 95 wt% of the binding liquid was 1.72. For the ink with 10 wt% iron oxide to 90 wt% of the binding liquid the Z number was 1.57. Both these values sit within the reported printable Z number range of $1 > Z > 10$.

The permittivity of the passive and active inks at a frequency of 8–12 GHz were 2.25 and 2.73 F/m, respectively. The real permittivity of the waffle structure was 2.65 F/m which showed intermediate properties between the two parent inks. Those results were also reverse-engineered to compute the electromagnetic properties of the materials which showed good agreement with the experimental work.

Printing the active inks was demonstrated successfully using a dual-head PixDro LP50 inkjet printer. A UV LED was attached to the print-head to cure the ink as it was deposited. This approach of mixing nanoparticles with a UV curable binding liquid is believed to allow for further development of functional inks that can be cured

using a UV light, and demonstrates the versatility of inkjet printing to include 3D structures of functional materials.

Acknowledgement

The authors gratefully acknowledge funding support from the UK DSTL (Defense Science and Technology Laboratory) under the SMART3D project, and the facility provided by EPSRC (Engineering and Physical Sciences Research Council) under the Jetting Electronic Tracks JET project, and the EPSRC Centre for Innovative Manufacturing in Additive Manufacturing (EP/I033335/2) at the University of Nottingham.

References

[1] J.B. Pendry, A.J. Holden, W.J. Stewart, I. Youngs, Extremely low frequency plasmons in metallic mesostructures, Phys. Rev. Lett. 76 (25) (1996) 4773–4776.
[2] D. Schurig, J.J. Mock, B.J. Justice, S.A. Cummer, J.B. Pendry, A.F. Starr, D.R. Smith, Metamaterial electromagnetic cloak at microwave frequencies, Science 314 (5801) (2006) 977–980.
[3] C.-J. Li, B. Wang, J.-N. Wang, Magnetic and microwave absorbing properties of electrospun Ba(1-x)LaxFe12O19 nanofibers, J. Magn. Magn. Mater. 324 (7) (2012) 1305–1311.
[4] E. Saleh, C. Tuck, C. Thiantanukij, P. Woolliams, B. Clarke, R. Wildman, I. Ashcroft, R. Hague, P. Dickens, 3D Inkjet-printed UV-curable Inks for Multi-functional Electromagnetic Applications, International Symposium on Flexible Automation, Japan, 2014, pp. 94L.
[5] J.R. Tumbleston, D. Shirvanyants, N. Ermoshkin, R. Janusziewicz, A.R. Johnson, D. Kelly, K. Chen, R. Pinschmidt, J.P. Rolland, A. Ermoshkin, E.T. Samulski, J.M. DeSimone, Continuous liquid interface production of 3D objects, Science 347 (6228) (2015) 1349–1352.
[6] J.J. Adams, E.B. Duoss, T.F. Malkowski, M.J. Motala, B.Y. Ahn, R.G. Nuzzo, J.T. Bernhard, J.A. Lewis, Conformal printing of electrically small antennas on three-dimensional surfaces, Adv. Mater. 23 (11) (2011) 1335–1340.
[7] J.A. Lewis, B.Y. Ahn, Device fabrication: three-dimensional printed electronics, Nature 518 (7537) (2015) 42–43.
[8] T. Kawase, H. Sirringhaus, R.H. Friend, T. Shimoda, Inkjet printed via-hole interconnections and resistors for all-polymer transistor circuits, Adv. Mater. 13 (21) (2001) 1601–1605.
[9] A. Kwas, E. MacDonald, C.J. Kief, R. Wicker, C. Soto, L. Bañuelos, J. Aarestad, B. Zufelt, J.D. Stegeman, C. Tolbert, Printing Multi-Functionality: Additive Manufacturing for CubeSats AIAA SPACE 2014 Conference and Exposition, American Institute of Aeronautics and Astronautics, 2014.
[10] L.E. Murr, E. Martinez, X. Pan, C. Meng, J. Yang, S. Li, F. Yang, Q. Xu, J. Hernandez, W. Zhu, S.M. Gaytan, F. Medina, R.B. Wicker, Microstructures and properties of solid and reticulated mesh components of pure iron fabricated by electron beam melting, J. Mater. Res. Technol. 2 (4) (2013) 376–385.
[11] E. Macdonald, R. Salas, D. Espalin, M. Perez, E. Aguilera, D. Muse, R.B. Wicker, 3D printing for the rapid prototyping of structural electronics, IEEE Access 2 (2014) 234–242.
[12] S.I. Zoltan, Pulsed Droplet Ejecting System, Google Patents, 1972.
[13] W.G. Hawkins, Bubble Jet Printing Device, Google Patents, 1985.
[14] H.P. Le, Progress and trends in ink-jet printing technology, J. Imaging Sci. Technol. 42 (1) (1998) 49–62.
[15] B. Derby, Inkjet printing of functional and structural materials: fluid property requirements, feature stability, and resolution, Annu. Rev. Mater. Res. 40 (1) (2010) 395–414.
[16] F. Zhang, C. Tuck, R. Hague, Y. He, E. Saleh, Y. Li, C. Sturgess, R. Wildman, Inkjet printing of polyimide insulators for the 3D printing of dielectric materials for microelectronic applications, J. Appl. Polym. Sci. 133 (18) (2016).
[17] H. Sirringhaus, T. Kawase, R.H. Friend, T. Shimoda, M. Inbasekaran, W. Wu, E.P. Woo, High-resolution inkjet printing of all-polymer transistor circuits, Science 290 (5499) (2000) 2123–2126.
[18] S.B. Walker, J.A. Lewis, Reactive silver inks for patterning high-conductivity features at mild temperatures, J. Am. Chem. Soc. 134 (3) (2012) 1419–1421.
[19] A.L. Dearden, P.J. Smith, D.-Y. Shin, N. Reis, B. Derby, P. O'Brien, A low curing temperature silver ink for use in ink-jet printing and subsequent production of conductive tracks, Macromol. Rapid Commun. 26 (4) (2005) 315–318.
[20] P.J. Smith, D.Y. Shin, J.E. Stringer, B. Derby, N. Reis, Direct ink-jet printing and low temperature conversion of conductive silver patterns, J. Mater. Sci. 41 (13) (2006) 4153–4158.
[21] H.K. Seung, P. Heng, P.G. Costas, K.L. Christine, M.J.F. Jean, P. Dimos, All-inkjet-printed flexible electronics fabrication on a polymer substrate by low-temperature high-resolution selective laser sintering of metal nanoparticles, Nanotechnology 18 (34) (2007) 345202.
[22] B.Y. Ahn, E.B. Duoss, M.J. Motala, X. Guo, S.-I. Park, Y. Xiong, J. Yoon, R.G. Nuzzo, J.A. Rogers, J.A. Lewis, Omnidirectional printing of flexible, stretchable, and spanning silver microelectrodes, Science 323 (5921) (2009) 1590–1593.
[23] X. Nie, H. Wang, J. Zou, Inkjet printing of silver citrate conductive ink on PET substrate, Appl. Surf. Sci. 261 (0) (2012) 554–560.
[24] E. Saleh, B. Liu, J.L. Fernandez, C. Tuck, R. Wildman, I. Ashcroft, R. Hague, P. Dickens, The optimization of conductive inks for 3D inkjet printing, NIP & Digital Fab. Conf. 2014 (1) (2014) 137–139.
[25] B.J. de Gans, P.C. Duineveld, U.S. Schubert, Inkjet printing of polymers: state of the art and future developments, Adv. Mater. 16 (3) (2004) 203–213.
[26] E.A. Sanchez, M. Waldmann, C.B. Arnold, Chalcogenide glass microlenses by inkjet printing, Appl. Opt. 50 (14) (2011) 1974–1978.
[27] J.-P. Lu, W.-K. Huang, F.-C. Chen, Self-positioning microlens arrays prepared using ink-jet printing, OPTICE 48 (7) (2009) (073606-073606-3).
[28] A.L. Hart, A.P.F. Turner, D. Hopcroft, On the use of screen- and ink-jet printing to produce amperometric enzyme electrodes for lactate, Biosens. Bioelectron. 11 (3) (1996) 263–270.
[29] E.A. Roth, T. Xu, M. Das, C. Gregory, J.J. Hickman, T. Boland, Inkjet printing for high-throughput cell patterning, Biomaterials 25 (17) (2004) 3707–3715.
[30] L. Setti, A. Fraleoni-Morgera, B. Ballarin, A. Filippini, D. Frascaro, C. Piana, An amperometric glucose biosensor prototype fabricated by thermal inkjet printing, Biosens. Bioelectron. 20 (10) (2005) 2019–2026.
[31] M.S. Mannoor, Z. Jiang, T. James, Y.L. Kong, K.A. Malatesta, W.O. Soboyejo, N. Verma, D.H. Gracias, M.C. McAlpine, 3D printed bionic ears, Nano Lett. 13 (6) (2013) 2634–2639.
[32] A. Goyanes, J. Wang, A. Buanz, R. Martínez-Pacheco, R. Telford, S. Gaisford, A.W. Basit, 3D Printing of medicines: engineering novel oral devices with unique design and drug release characteristics, Mol. Pharm. 12 (11) (2015) 4077–4084.
[33] I. Yuzo, K. Shinji, A. Yoshimitsu, A. Yasuhiro, Ink-Jet fabrication of polymer microlens for optical-I/O chip packaging, Jpn. J. Appl. Phy. 39 (3S) (2000) 1490.
[34] J.Y. Kim, N.B. Brauer, V. Fakhfouri, D.L. Boiko, E. Charbon, G. Grutzner, J. Brugger, Hybrid polymer microlens arrays with high numerical apertures fabricated using simple ink-jet printing technique, Opt. Mater. Express 1 (2) (2011) 259–269.
[35] M. Sangermano, A. Chiolerio, G. Marti, P. Martino, UV-cured acrylic conductive inks for microelectronic devices, Macromol. Mater. Eng. 298 (6) (2013) 607–611.
[36] A. Chiolerio, M. Sangermano, In situ synthesis of Ag-acrylic nanocomposites: tomography-based percolation model, irreversible photoinduced electromigration and reversible electromigration, Mater. Sci. Eng. B 177 (4) (2012) 373–380.
[37] G.A. Gelves, B. Lin, U. Sundararaj, J.A. Haber, Low electrical percolation threshold of silver and copper nanowires in polystyrene composites, Adv. Funct. Mater. 16 (18) (2006) 2423–2430.
[38] H. Song, J. Spencer, A. Jander, J. Nielsen, J. Stasiak, V. Kasperchik, P. Dhagat, Inkjet printing of magnetic materials with aligned anisotropy, J. Appl. Phys. 115 (17) (2014) 17E308.
[39] T. Nardi, M. Sangermano, Y. Leterrier, P. Allia, P. Tiberto, J.-A.E. Månson, UV-cured transparent magnetic polymer nanocomposites, Polymer 54 (17) (2013) 4472–4479.
[40] L. Jacot-Descombes, M. Gullo, V. Cadarso, M. Mastrangeli, O. Ergeneman, C. Peters, P. Fatio, M. Freidy, C. Hierold, B. Nelson, J. Brugger, Inkjet printing of high aspect ratio superparamagnetic su-8 microstructures with preferential magnetic directions, Micromachines 5 (3) (2014) 583.
[41] P.S. Grant, F. Castles, Q. Lei, Y. Wang, J.M. Janurudin, D. Isakov, S. Speller, C. Dancer, C.R.M. Grovenor, Manufacture of electrical and magnetic graded and anisotropic materials for novel manipulations of microwaves, Philosophical transactions, Ser. A Math. Phys. Eng. Sci. 373 (2049) (2015) 20140353.
[42] C.M. Shemelya, A. Rivera, A.T. Perez, C. Rocha, M. Liang, X. Yu, C. Kief, D. Alexander, J. Stegeman, H. Xin, R.B. Wicker, E. MacDonald, D.A. Roberson, Mechanical, electromagnetic, and X-ray shielding characterization of a 3D printable tungsten-polycarbonate polymer matrix composite for space-based applications, J. Electron. Mater. 44 (8) (2015) 2598–2607.
[43] W.V. Ohnesorge, Die Bildung von Tropfen an Düsen und die Auflösung flüssiger Strahlen, ZAMM J. Appl. Math. Mech./Zeitschrift für Angewandte Mathematik und Mechanik 16 (6) (1936) 355–358.
[44] T. Jiayan, G. Hiong Yap, L. Yen Nan, L. Boon Keng, Control of droplet formation in inkjet printing using ohnesorge number category: materials and processes, electronics packaging technology conference, 2008, EPTC 2008. 10th (2008) 761–766.
[45] D. Jang, D. Kim, J. Moon, Influence of fluid physical properties on ink-jet printability, Langmuir 5 (5) (2009) 2629–2635.
[46] N. Reis, C. Ainsley, B. Derby, Ink-jet delivery of particle suspensions by piezoelectric droplet ejectors, J. Appl. Phys. 97 (9) (2005) 094903.
[47] K.A.M. Seerden, N. Reis, J.R.G. Evans, P.S. Grant, J.W. Halloran, B. Derby, Ink-jet printing of wax-based alumina suspensions, J. Am. Ceram. Soc. 84 (11) (2001) 2514–2520.
[48] R.N. Clarke, A.P. Gregory, D. Cannell, M. Patrick, S. Wylie, I. Youngs, G. Hill, A Guide to the Characterisation of Dielectric Materials at Rf and Microwave Frequencies, British Library, London, 2003.
[49] C. Smartt, S. Greedy, Time Domain electromagnetic modelling based on the TLM technique. <https://github.com/ggiemr/GGI_TLM> (accessed 11.11.15).
[50] C. Christopoulos, The Transmission-Line Modeling Method: TLM, Wiley-IEEE Press, 1996.